

Efficient Fine-Tuning of Quantized Models via Adaptive Rank and Bitwidth

Changhai Zhou

Fudan University
zhouch23@m.fudan.edu.cn

Shijie Han

Columbia University
sh4460@columbia.edu

Shiyang Zhang

Columbia University
sz3209@columbia.edu

Yuhua Zhou

Zhejiang University
zhouyuhua@zju.edu.cn

Weizhong Zhang

Fudan University
weizhongzhang@fudan.edu.cn

Cheng Jin

Fudan University
jc@fudan.edu.cn

Abstract

As large language models (LLMs) scale up, model compression becomes crucial for resource-constrained deployment. While QLoRA reduces resource demands via parameter quantization and LoRA fine-tuning, its uniform-precision quantization limits performance by ignoring parameter importance variations. Dynamic mixed-precision strategies adaptively adjust quantization bitwidth based on parameter sensitivity, and dynamic LoRA mechanisms enhance quantized model adaptation. Existing works separately optimize dynamic quantization or LoRA parameters, leaving their synergistic integration as an unresolved core challenge. To address this, we propose **QR-Adaptor**, a unified, gradient-free strategy that uses partial calibration data to jointly search the quantization components and the rank of low-rank spaces for each layer, thereby continuously improving model performance. QR-Adaptor does not minimize quantization error but treats precision and rank allocation as a discrete optimization problem guided by actual downstream performance and memory usage. Compared to state-of-the-art (SOTA) quantized LoRA fine-tuning methods, our approach achieves a 4.89% accuracy improvement on average, and in some cases even outperforms the 16-bit fine-tuned model while maintaining the memory footprint of the 4-bit setting.

1 Introduction

Large Language Models (LLMs) have achieved remarkable success in both language understanding and generation [Makridakis et al., 2023, Raiaan et al., 2024, Chang et al., 2024], yet adapting these powerful models to specific downstream tasks is often hindered by immense computational and memory costs [Wan et al., 2023]. Parameter-Efficient Fine-Tuning (PEFT) methods, such as Low-Rank Adaptation (LoRA) [Hu et al., 2022], address these bottlenecks by introducing lightweight low-rank updates to the core model parameters, thereby reducing the storage and compute needed for full gradient-based optimization. In parallel, quantization techniques [Gong et al., 2014, Gupta et al., 2015] compress weight matrices to fewer bits, enabling faster inference and lower memory footprints. Building on these two lines of research, QLoRA [Dettmers et al., 2023] has become a widely adopted paradigm for memory-efficient LLM fine-tuning, effectively pairing quantization with LoRA.

Recent works aim to further reduce quantization errors by adjusting the quantized weights before fine-tuning. For instance, LoftQ [Li et al., 2023] fits a portion of the error $\mathbf{W} - \mathbf{Q}$ through SVD-based initialization, and LQ-LoRA [Guo et al., 2024] attempts a similar correction strategy. While these approaches can boost performance after *one* iteration, multiple iterative corrections sometimes degrade accuracy, as illustrated in Figure 1, where LoftQ performance declines over several rounds. This drop arises in part from a mismatch between the discrete nature of quantization and continuous SVD updates, which risk shifting the model away from both \mathbf{Q} and \mathbf{W} . Additionally, methods that dynamically adjust LoRA’s rank at run time, such as AdaLoRA [Zhang et al., 2023b], may introduce extra complexity for quantized models whose robustness has already been weakened [Gong et al., 2024].

We introduce **QR-Adaptor**, an approach that aims to circumvent these shortcomings by exploring each layer’s bitwidth and LoRA level in a uniform search space. Rather than optimizing quantization and LoRA parameters in isolation—or iteratively refining continuous residuals—QR-Adaptor jointly determines each layer’s precision level (q_l) and adaptation capacity (r_l). This approach exploits the interplay between numerical precision and low-rank expressiveness: certain layers may demand a higher bit-width to preserve critical features, while others benefit more from an increased LoRA rank to capture complex task-specific cues. By considering both factors together, QR-Adaptor achieves more robust control over memory usage and downstream accuracy. Specifically, our method conducts a *gradient-free*, multi-objective search over discrete (q_l, r_l) pairs for each layer. To keep the computational burden comparable to a single SVD iteration, we evaluate candidate configurations only on a small *partial calibration* subset of the training data. Through this design, QR-Adaptor avoids the shortcomings of iterative SVD-based error fitting and leverages a cohesive search strategy that systematically aligns quantization precision with LoRA’s representational power in quantized LLM fine-tuning.

To robustly navigate the high-dimensional configuration space, QR-Adaptor adopts a three-stage optimization pipeline. It begins with a **task-informed initialization**, estimating each layer’s relative importance via an entropy-based criterion rather than gradient heuristics. This guides the allocation of quantization bit-widths and LoRA ranks, narrowing the search to promising configurations. Building on this, we conduct a **global exploration** using a Pareto-ranking genetic algorithm reminiscent of NSGA-II Deb et al. [2002] to maintain diversity across the performance–memory trade-off. Finally, we apply **local refinement** with Bayesian optimization, efficiently identifying optimal configurations. This systematic integration mitigates the limitations of iterative error-fitting and consistently outperforms baseline approaches in both accuracy and adaptability. We summarize our main contributions as follows:

- We uncover the reasons why existing iterative methods, which focus on reducing quantization errors through continuous optimization, fail to consistently enhance the performance of quantized models. In particular, we find that merely refining SVD-based corrections or individually adjusting bit-widths or LoRA ranks cannot adequately boost the capabilities of quantized LLMs.
- We propose a multi-objective, gradient-free optimization strategy, **QR-Adaptor**, which jointly searches for the per-layer bit-width and LoRA rank. This approach integrates task-informed initialization, a Pareto-ranking genetic algorithm, and Bayesian optimization, and keeps the overhead comparable to a single SVD iteration by using calibration data.
- Our method consistently outperforms previous baselines on multiple benchmarks (e.g., achieving a 4.89% improvement in accuracy on GSM8K). In some cases, it even surpasses 16-bit fine-tuned models while requiring memory comparable to that of a 4-bit setting.

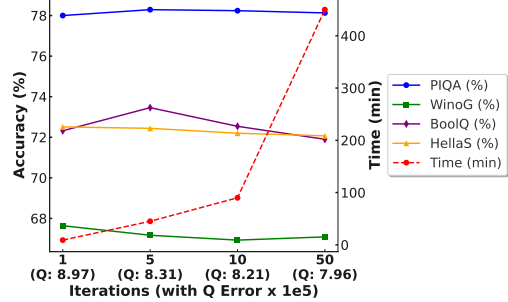


Figure 1: LoftQ iterations, quantization error, fine-tuning performance, and time cost. As the iteration count increases, the overall quantization error slightly decreases but does not yield proportional boosts in downstream performance. Moreover, the fraction of the error that can still be reduced shrinks with each iteration, ultimately fitting around 20% of the quantization error.

2 Background

In this section, we analyze why iterative methods that aim to reduce quantization errors via continuous SVD-based updates can be suboptimal when weights are constrained to a discrete lattice. We also provide optimization paths for three different fine-tuned initialization strategies in Appendix A, illustrating that iterative fitting of quantization errors may not be able to approximate the original accuracy model, thus motivating our proposed approach.

2.1 Discrete Nature of Quantization

Definition 2.1 (Quantization Operator). For a weight matrix $\mathbf{W} \in \mathbb{R}^{d \times k}$ and quantization step Δ , the quantization operator is defined as:

$$\text{Quantize}(\mathbf{W}) = \Delta \cdot \left\lfloor \frac{\mathbf{W}}{\Delta} + \frac{1}{2} \right\rfloor, \quad (1)$$

where $\lfloor \cdot \rfloor$ denotes element-wise rounding. This operation projects \mathbf{W} onto the discrete lattice:

$$\mathcal{L} = \Delta \cdot \mathbb{Z}^{d \times k} \subset \mathbb{R}^{d \times k}. \quad (2)$$

Interpretation. This formalizes that each parameter in \mathbf{W} can only take values from a discrete set (the “lattice”) after quantization. Even small changes in real-valued space may map to the *same* discrete point under rounding, causing discontinuities in any gradient-based updates.

2.2 Mismatch in Continuous Approximations

Existing methods often minimize

$$\min_{\mathbf{A}, \mathbf{B}} \left\| \mathbf{W} - \underbrace{\text{Quantize}(\mathbf{W})}_{\in \mathcal{L}} - \mathbf{AB} \right\|_F. \quad (3)$$

However, this objective presumes a continuous measure of error (the Frobenius norm) even though the feasible set $\text{Quantize}(\mathbf{W})$ is discrete.

Key Issues.

- *Space Duality:* The solution space for \mathbf{AB} is continuous ($\mathbb{R}^{d \times r} \times \mathbb{R}^{r \times k}$), whereas $\text{Quantize}(\mathbf{W})$ must remain in the discrete lattice \mathcal{L} . Thus, $\text{Quantize}(\mathbf{W}) + \mathbf{AB}$ might lie outside \mathcal{L} after updates, negating any continuous gains.
- *Gradient Discontinuity:* Let $\mathcal{P}_{\mathcal{L}}$ project onto \mathcal{L} . True gradient flow would require differentiating through $\mathcal{P}_{\mathcal{L}}(\text{Quantize}(\mathbf{W}) + \mathbf{AB})$. But $\mathcal{P}_{\mathcal{L}}$ has zero gradient *almost everywhere*, making standard backpropagation ineffective for adjusting \mathbf{AB} in a discrete context.

Implication. Because $\mathbf{Q} = \text{Quantize}(\mathbf{W})$ is fixed to a discrete set, continuously optimizing \mathbf{A}, \mathbf{B} to reduce $\|\mathbf{W} - \mathbf{Q} - \mathbf{AB}\|_F$ can yield diminishing or no improvements in final performance. Each step might look beneficial in a continuous sense but fails to move to a truly better discrete state.

2.3 Formal Proof of Suboptimality

Proposition 2.2. *Let*

$$\mathbf{AB}^* = \arg \min_{\mathbf{A}, \mathbf{B}} \left\| \mathbf{W} - \text{Quantize}(\mathbf{W}) - \mathbf{AB} \right\|_F. \quad (4)$$

Then there exists a $\mathbf{Q}' \in \mathcal{L}$ such that

$$\|\mathbf{W} - \mathbf{Q}'\|_F < \|\mathbf{W} - \text{Quantize}(\mathbf{W}) - \mathbf{AB}^*\|_F. \quad (5)$$

Proof. By the projection theorem:

$$\|\mathbf{W} - \mathcal{P}_{\mathcal{L}}(\mathbf{W})\|_F \leq \|\mathbf{W} - \mathbf{X}\|_F \quad \forall \mathbf{X} \in \mathcal{L}, \quad (6)$$

$$\|\mathbf{W} - \mathbf{Q}'\|_F \leq \|\mathbf{W} - \text{Quantize}(\mathbf{W}) - \mathbf{AB}^*\|_F, \quad (7)$$

where $\mathbf{Q}' = \mathcal{P}_{\mathcal{L}}(\mathbf{W})$. Equality holds only if $\text{Quantize}(\mathbf{W}) + \mathbf{AB}^* \in \mathcal{L}$, requiring \mathbf{AB}^* to exactly compensate discrete rounding errors—an event with measure zero in high dimensions. \square

Interpretation. This proposition states that even the best continuous low-rank correction \mathbf{AB}^* *cannot* fully offset the errors introduced by discrete quantization. A strictly better discrete point \mathbf{Q}' often exists in lattice space, demonstrating that methods trying to fix $\text{Quantize}(\mathbf{W})$ plus a real-valued \mathbf{AB} can remain suboptimal. In simpler terms, *no matter how well we approximate $\mathbf{W} - \text{Quantize}(\mathbf{W})$ by a continuous matrix, there may be a better purely discrete solution.*

2.4 Manifold Analysis

We can decompose the parameter space as

$$\mathcal{M} = \mathcal{L} \oplus \{\mathbf{AB} \mid \text{rank}(\mathbf{AB}) \leq r\}. \quad (8)$$

Because \mathcal{L} is discrete and $\{\mathbf{AB}\}$ is continuous, their sum \mathcal{M} is a hybrid space.

Critical Observations.

- The intersection $\mathcal{L} \cap (\text{Quantize}(\mathbf{W}) + \{\mathbf{AB}\})$ forms isolated points, underscoring the *rare alignment* needed for continuous \mathbf{AB} to fix discrete rounding completely.
- The effective search space $\mathcal{M}_{\text{eff}} = \{\mathcal{P}_{\mathcal{L}}(\text{Quantize}(\mathbf{W}) + \mathbf{AB})\}$ has a fractal-like structure, reflecting the discontinuous jumps among discrete levels.

Implication. As dimension $d \times k$ grows, the measure of \mathbf{AB} that perfectly lands in the same discrete cell as \mathbf{W} becomes negligible. This reinforces the statement that *purely continuous approximations rarely coincide with actual quantized solutions*, making Frobenius-based SVD updates unreliable for improving final performance.

2.5 Dynamical System Perspective

Training dynamics can be modeled by

$$\frac{d}{dt} \begin{pmatrix} \mathbf{A} \\ \mathbf{B} \end{pmatrix} = -\eta \nabla_{\mathbf{A}, \mathbf{B}} \mathcal{L}(\mathcal{P}_{\mathcal{L}}(\text{Quantize}(\mathbf{W}) + \mathbf{AB})). \quad (9)$$

Key Properties.

- The right-hand side is piecewise constant, with jumps on the boundaries of \mathcal{L} . Small changes in \mathbf{A}, \mathbf{B} that do not cross a boundary in \mathcal{L} produce no difference in the discrete projection.
- Eigenvalues of the Jacobian vanish when projected onto the interior of a lattice cell. This means typical continuous gradient-based methods cannot easily escape suboptimal cells since they see "flat" gradients within each cell.

Meaning for Practical Fine-Tuning. This piecewise constant nature implies that *iterative SVD or gradient-based fitting* will exhibit plateau-like behavior in large regions, only changing when crossing quantization boundaries. Consequently, even if $\|\mathbf{W} - (\mathbf{Q} + \mathbf{AB})\|_F$ looks partially improved in a real-valued sense, the *actual* quantized weights remain stuck. Hence, iterative error-fitting procedures may end up stagnating.

Collectively, these findings explain why repeated SVD-based steps may reduce the *continuous* norm $\|\mathbf{W} - \mathbf{Q}\|_F$, yet fail to yield stable accuracy improvements under quantization. In contrast, our approach (Section 3) avoids this pitfall by adopting a *gradient-free, multi-objective* strategy. Instead of directly minimizing Frobenius error in a continuous space, we evaluate each candidate (bit-width, LoRA rank) *within* the discrete quantized domain to optimize real downstream performance and memory usage.

3 Methodology

3.1 Problem Formulation

We consider a pre-trained LLM of L layers. Each layer l has a base weight matrix $\mathbf{W}_l \in \mathbb{R}^{d \times k}$, which we wish to *both* quantize to a lower bit-width q_l *and* augment with a low-rank LoRA adaptation

of rank r_l . Specifically, let

$$q_l \in \mathcal{Q} \quad \text{and} \quad r_l \in \mathcal{R},$$

where \mathcal{Q} is the set of all feasible bit-width values (e.g., 4, 8 bits) and \mathcal{R} the set of all feasible LoRA ranks. We unify these layer-wise assignments into a single *configuration*:

$$C = \{(q_1, r_1), (q_2, r_2), \dots, (q_L, r_L)\},$$

and let \mathcal{C} be the space of all such configurations.

Layer-wise Quantization & LoRA. For layer l , we apply a *quantization function* to obtain:

$$\hat{\mathbf{W}}_l^{q_l} = \text{Quantize}(\mathbf{W}_l, q_l). \quad (10)$$

We then add a *low-rank* term $\Delta \mathbf{W}_l^{r_l} = \mathbf{A}_l \mathbf{B}_l$, where $\mathbf{A}_l \in \mathbb{R}^{d \times r_l}$ and $\mathbf{B}_l \in \mathbb{R}^{r_l \times k}$. The layer’s forward pass for an input $\mathbf{x} \in \mathbb{R}^k$ is:

$$\mathbf{y} = \hat{\mathbf{W}}_l^{q_l} \mathbf{x} + \Delta \mathbf{W}_l^{r_l} \mathbf{x}. \quad (11)$$

Hence, each layer’s parameters become a combination of discrete weights $\hat{\mathbf{W}}_l^{q_l}$ (bit-width q_l) and a continuous LoRA update of rank r_l .

Objective: Performance vs. Memory. Our goal is to find a configuration $C \in \mathcal{C}$ that yields high accuracy on a training set $\mathcal{D}_{\text{train}}$ (evaluated on downstream tasks $\mathcal{D}_{\text{test}}$) while minimizing memory usage. Let $P(C)$ be the model’s performance under configuration C , and let $M(C)$ be its total memory footprint (including quantized weights and LoRA parameters). We combine these criteria in a single weighted objective:

$$\begin{aligned} \max_{C \in \mathcal{C}} \quad & \alpha \frac{P(C) - \mu_P}{\sigma_P} - (1 - \alpha) \frac{M(C) - \mu_M}{\sigma_M}, \\ \text{subject to} \quad & q_l \in \mathcal{Q}, r_l \in \mathcal{R}, \text{ for each } l = 1, \dots, L. \end{aligned} \quad (12)$$

Here, (μ_P, σ_P) and (μ_M, σ_M) are the mean and standard deviation of performance and memory, computed over sample configurations to normalize their scales. The parameter $\alpha \in [0, 1]$ governs the trade-off: a larger α places more emphasis on performance $P(C)$, whereas a smaller α prioritizes memory reduction $M(C)$.

3.2 QR-Adaptor Framework

Our approach differs from previous methods relying on fixed or hierarchical dynamic single configurations. We jointly explore the configuration space of quantization bits and LoRA ranks, creating a comprehensive search space that encompasses all potential optimal configurations. The main challenges in implementing this gradient-free optimization process are (a) The high-dimensional, discrete nature of the configuration space. (b) The computational cost of evaluating performance. To address these challenges, we propose QR-Adaptor, a method that effectively finds the relative optimal solution in three stages.

Task Information Based Initialization Our optimization pipeline starts by estimating the *relative importance* of each layer to the downstream task. Rather than relying on gradient norms (which may fail to capture a layer’s true influence on inference), we adopt an *information-entropy* criterion:

$$I(l) = H(Y) - H(Y | X_l), \quad (13)$$

where $H(Y)$ is the entropy of the model’s outputs, and $H(Y | X_l)$ is the conditional entropy given the l -th layer’s intermediate representation. Layers with a higher $I(l)$ exert greater impact on final predictions. Empirically, we find (Appendix G.1) that this entropy-based approach outperforms gradient-norm heuristics in selecting effective layers for bit-width and rank adjustments.

We initialize per-layer quantization bits $\{q_l\}$ by assigning larger q_l to layers with higher importance scores and smaller q_l to those deemed less critical. After quantizing the model with these initial bits, we recompute layer importance under quantization and then allocate LoRA ranks $\{r_l\}$: layers that remain most vital post-quantization receive larger r_l , while others get reduced ranks. This two-step procedure narrows the search space to promising configurations from the outset, guiding subsequent multi-objective optimization toward higher accuracy and lower memory usage.

Global Exploration with PRGA In LLM fine-tuning, quantization bits and LoRA ranks can be viewed as genetic traits, with performance and memory usage as phenotypic outcomes. Inspired by NSGA-II Deb et al. [2002], we propose PRGA (Pareto Ranking Genetic Algorithm), a multi-objective optimization method that jointly explores bit-rank configurations to balance performance and memory. Each configuration is represented as $C = (q_l, r_l)_{l=1}^L$, where q_l and r_l are the quantization bit and LoRA rank for layer l . PRGA evolves a population using elitist selection, crossover, and mutation, optimizing toward a Pareto frontier of trade-offs between accuracy and memory. The process continues until a stopping criterion or iteration limit is reached.

Before presenting the PRGA workflow, we introduce key concepts in multi-objective minimization. Given n objective functions $f_i(x), i = 1, \dots, n$, we say a solution X_a dominates X_b if $f_i(X_a) \leq f_i(X_b)$ for all i , with strict inequality for at least one i . A non-dominated solution is one not dominated by any other in the set. Pareto rank classifies solutions based on dominance: rank 1 includes all non-dominated solutions; removing them reveals the next layer of non-dominated solutions (rank 2), and so on, until all solutions are ranked.

As illustrated in Algorithm 1, we employ the Pareto Ranking to sort all individuals within the population. To address solutions with identical Pareto ranks, we use the crowding distance d for further differentiation within each Pareto rank. The detailed calculation of the crowding distance is presented in Algorithm 2.

Elite retention simulates natural selection by preserving top-performing individuals after evaluating Pareto rank and crowding distance. We first merge parent and offspring populations, then build the next generation by sequentially adding individuals from the lowest Pareto rank upward. If a rank cannot be fully included, individuals in that layer are sorted by crowding distance (descending), and the most diverse are selected until the population reaches capacity. Crossover and mutation follow Simulated Binary Crossover (SBX) and Polynomial Mutation, adapted for L pairs of integers (q_l, r_l) . Detailed procedures are shown in Algorithm 3 and Algorithm 4. These operations enable effective exploration and refinement of bit-rank configurations.

As shown in Figure 2, PRGA begins by generating an initial population of size N through randomization from prior configurations. It iteratively applies selection, crossover, and mutation to create offspring, merges them with parents, fine-tunes each individual on a validation subset, and evaluates their performance and memory. Pareto ranks and crowding distances are used to select the next generation, and the cycle repeats until convergence, yielding a Pareto frontier of optimal trade-offs.

Local Refinement with Bayesian Optimization While PRGA effectively explores the global configuration space, it may miss fine-grained local optima near the Pareto front. To address this, we apply Bayesian optimization, which excels at optimizing expensive black-box functions with uncertainty quantification. We begin by using the PRGA-derived Pareto front as initial samples. Each configuration is quickly fine-tuned and evaluated for actual performance and memory usage. These results are used to compute a weighted objective value y (per Equation 12), based on user-defined preferences. The y values, along with the RBF kernel-based covariance matrix K , are used to build a Gaussian process model. This model both quantifies uncertainty and guides the search toward the best-performing point for further refinement.

The next phase involves employing a random search strategy to select new sampling points in the vicinity of this top-performing configuration. For each newly selected sampling point x^* , we leverage the Gaussian process to estimate its predicted value and uncertainty using the following equations:

$$\begin{aligned}\mu(x^*) &= m(x^*) + K(x^*, X)K(X, X)^{-1}(y - m(X)) \\ \sigma^2(x^*) &= k(x^*, x^*) - K(x^*, X)K(X, X)^{-1}K(X, x^*)\end{aligned}\tag{14}$$

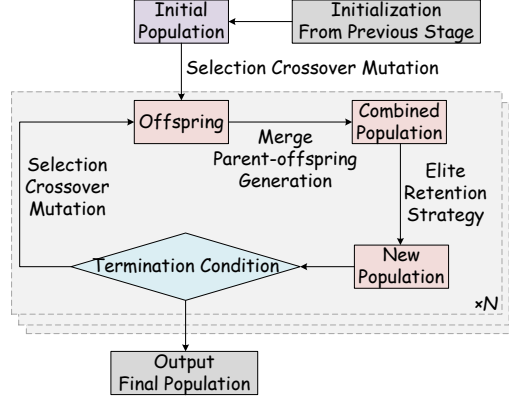


Figure 2: Detailed PRGA flow chart. The input is a set of solutions from the initialization, and the output is a set of Pareto front solutions containing multiple solutions.

where $m(x^*)$ is the prior mean function, $K(x^*, X)$ is the covariance between the new point and the existing points, and $K(X, X)$ is the covariance matrix of the existing points.

We then employ the Expected Improvement (EI) as the acquisition function, calculating it using the following formula:

$$EI(x^*) = \sigma(x^*) (Z \cdot \Phi(Z) + \phi(Z))$$

$$\text{and } Z = \frac{\mu(x^*) - y_{\text{best}}}{\sigma(x^*)} \quad (15)$$

, where $\Phi(Z)$ is the cumulative distribution function of the standard normal distribution, while $\phi(Z)$ is its probability density function and y_{best} is the best objective value among all points.

We select the configuration with the highest Expected Improvement (EI) as the next evaluation point and quickly fine-tune the LLM using it. The resulting performance and memory usage are used to compute the objective value. If this new point outperforms the current best, it becomes the new optimum; otherwise, the search continues around the previous best. In either case, the new data point is added to the training set, and the Gaussian process model is updated before the next iteration. This process repeats until a stopping condition—such as iteration limit, convergence, or time constraint—is met. The full procedure is illustrated in Figure 3.

The final output of this Bayesian optimization phase is a refined set of high-quality configurations that better capture the trade-offs between performance and memory. These optimized solutions offer practitioners a practical set of choices tailored to their specific resource constraints and performance goals.

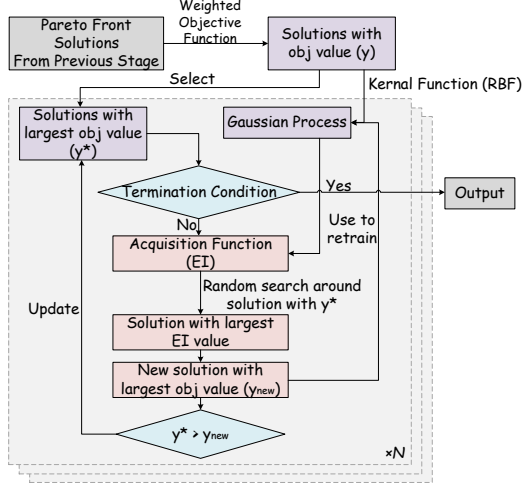


Figure 3: Detailed Bayesian optimization flow chart. Input is the Pareto front solution set from the global search, and output is a set of optimal solutions obtained according to the requirements.

4 Evaluation

In this section, we first introduce the experimental setup, including datasets, models, baselines, and implementation details. All hyperparameters aside from rank value and bit-width are kept consistent with the baselines.

4.1 Experimental Setup

Datasets and LLMs. We utilize the Alpaca52k and hc3 [Taori et al., 2023] for fine-tuning and evaluate the zero-shot performance of these LLMs on benchmarks including BoolQ [Clark et al., 2019], PIQA [Bisk et al., 2020], HellaSwag [Zellers et al., 2019], WinoGrande [Sakaguchi et al., 2021], ARC-easy [Clark et al., 2018], ARC-challenge [Clark et al., 2018], OpenbookQA [Mihaylov et al., 2018], and MMLU Hendrycks et al. [2021]. The models used in our experiments are Llama2 Touvron et al. [2023] and Llama3.1 Grattafiori et al. [2024].

Baselines. We compare our method against several baselines: without tuning, LoRA Hu et al. [2022], QLoRA Dettmers et al. [2023], Adalora Zhang et al. [2023b], LoftQ Li et al. [2023], and LQ-LoRA Guo et al. [2024]. We evaluated the performance of LoftQ with different iteration numbers. For Adalora, which dynamically allocates ranks based on the average rank budget, we set the budget to 8 and 64. Finally, for LQ-LoRA, which allocates quantization bit-width based on the average weight bit-width budget and quantization error, we set the bit-width budget to 4.

Implementation Details. We utilize the following configurations: *PyTorch* version 2.1.2, *Bit-sandBytes* library version 0.43.1, *Transformers* library version 4.41.0, *PEFT* library version 0.11.1,

Table 1: Performance comparison of different methods across various bit-width configurations on Llama3.1-8B. Superscripts on LoftQ bits indicate the number of initialization iterations. Bold figures represent the best performance for a given model and task, while underlined figures indicate the second-best. Accuracy is reported as %.

	Method	Bit	ARC(C)	ARC(E)	BoolQ	GSM8K	HellaS	OBQA	PIQA	WinoG	Average
Rank = 8	LoRA	16	56.14	83.88	83.18	54.36	79.44	45.20	82.10	75.30	69.95
	QLoRA	8	57.08	83.46	82.48	53.75	<u>79.63</u>	46.00	<u>82.10</u>	74.59	69.89
	QLoRA	4	54.35	82.41	82.08	44.35	78.82	44.20	81.50	73.64	67.67
	AdaLoRA	16	52.90	81.99	81.87	50.57	78.65	45.00	81.34	73.95	68.28
	AdaLoRA	8	52.90	81.86	82.05	49.96	78.65	44.80	81.34	74.43	68.25
	AdaLoRA	4	51.28	80.98	80.61	37.83	77.36	42.80	80.74	72.53	65.51
	LoftQ	4 ¹	54.86	82.74	82.26	51.40	78.65	46.00	81.45	73.24	68.82
	LoftQ	4 ⁵	52.65	81.82	81.53	39.65	78.50	43.40	81.39	72.69	66.45
	LoftQ	4 ¹⁰	51.88	81.31	79.66	38.44	78.01	43.20	81.12	71.98	65.70
	QR-Adaptor	5.45	<u>56.83</u>	84.12	83.38	56.29	80.93	<u>45.80</u>	82.92	<u>75.10</u>	70.67
Rank = 16	LoRA	16	56.74	83.63	83.00	54.13	<u>79.51</u>	44.40	81.83	74.43	69.70
	QLoRA	8	56.23	82.91	82.66	53.68	<u>79.46</u>	46.00	81.66	<u>74.74</u>	69.67
	QLoRA	4	53.84	81.99	82.11	44.66	78.76	44.40	81.72	73.09	67.57
	AdaLoRA	16	53.07	82.03	81.99	50.11	78.61	45.40	81.28	74.11	68.33
	AdaLoRA	8	53.33	82.03	82.11	49.13	78.57	45.20	81.34	73.79	68.19
	AdaLoRA	4	50.85	80.72	80.73	37.98	77.34	42.80	80.52	73.16	65.51
	LoftQ	4 ¹	55.12	82.58	82.69	49.81	78.82	<u>45.80</u>	81.28	74.27	68.80
	LoftQ	4 ⁵	53.92	82.32	81.56	42.00	78.54	43.80	81.56	72.77	67.06
	LoftQ	4 ¹⁰	52.90	81.69	81.56	39.88	78.64	43.80	81.07	71.98	66.44
	QR-Adaptor	5.45	56.83	84.12	83.38	56.29	80.93	<u>45.80</u>	82.92	75.10	70.67

Optuna library version 3.6.1, CUDA version 12.4, GPU: NVIDIA L20 GPU. Operating System: Ubuntu. Concise implementation details are provided in the Appendix F. We define the population size as 5 and generate 1 new offspring in each iteration. The second and third phases were iterated 5 times.

4.2 Main Results

We present the performance comparison of LLaMA3.1-8B on commonsense understanding tasks in Table 1. For practical deployment, we exclude the 2-bit configuration in mixed-precision setups, as it does not significantly reduce memory usage. Results with 2-bit configurations are shown in Appendix D.7. Our method achieves or surpasses the performance of 16-bit fine-tuned models while maintaining the same memory footprint as the 4-bit models.

As mentioned, LoftQ outperforms 4-bit QLoRA after one iteration, but its performance degrades with more iterations. This is due to the mismatch between continuous error correction and discrete quantization. AdaLoRA, which dynamically adjusts LoRA rank during fine-tuning, is less effective for quantized models, as the quantization process introduces discrete constraints incompatible with dynamic rank changes. Additional results for longer training epochs are available in Appendix D.6.

QR-Adaptor jointly optimizes bit-width and LoRA rank, balancing precision and adaptation capacity for superior performance. Our results confirm that jointly optimizing these parameters leads to better downstream performance. Furthermore, QR-Adaptor allocates resources more efficiently by assigning higher LoRA ranks to critical layers and higher precision to important layers, achieving high accuracy with low memory usage.

Due to space constraints, additional experimental results and analyses are provided in Appendix D, including: (1) extended results across different models (D.1, D.2, D.6, D.7); (2) evaluations on larger datasets with higher LoRA ranks (D.3); (3) training time comparisons (D.4); and (4) fair bit-width configuration comparisons (D.5).

4.3 Ablation Study

We use the WinoGrande benchmark to conduct an ablation study assessing the contribution of each stage in QR-Adaptor. As shown in Figure 4, removing either PRGA or Bayesian optimization leads to unbalanced search behavior—PRGA alone explores too broadly, while Bayesian optimization alone is overly narrow—reflecting their extrapolation and interpolation roles, respectively. Omitting

stage 1 causes PRGA to initiate from random configurations, resulting in scattered search patterns. Nonetheless, it still reaches the upper-left optimal region, highlighting the strength of PRGA and Bayesian optimization. In contrast, the full three-stage pipeline first explores broadly around a guided initialization, then refines near promising areas, yielding the best configurations.

Further ablation studies assess the impact of each stage by removing them individually and analyzing the resulting performance. We also perform sensitivity analysis on PRGA hyperparameters, with details provided in Appendix G.

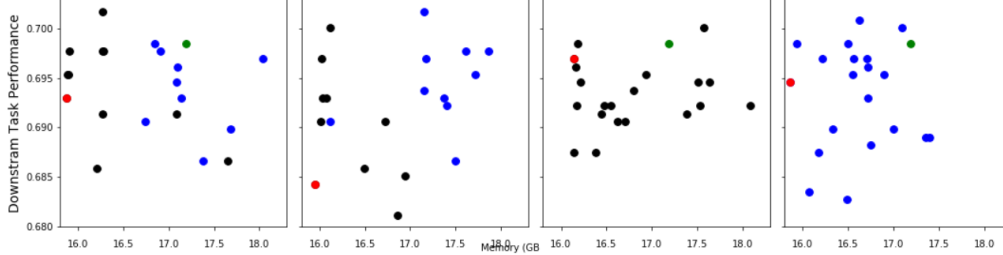


Figure 4: From left to right, the actual measured performance and memory usage of the configurations generated by QR-Adaptor, QR-Adaptor without stage1, QR-Adaptor without stage2, and QR-Adaptor without stage3 are shown. Different colors represent the configurations generated at different stages.

5 Related Work

LLM Quantization. The field of LLM quantization has witnessed substantial progress, driven by the need for efficient model deployment. Recent research has introduced several innovative approaches. Frantar et al. [2023] have developed GPTQ, which achieves 4-bit precision with layer-wise quantization. Lin et al. [2023] have proposed AWQ, which improves accuracy for heavily quantized models. Yao et al. [2022] have introduced ZeroQuant, which preserves zero-shot capabilities at lower bit widths. Dettmers et al. [2022] have presented LLM.int8(), which enables 8-bit quantization for consumer hardware. Kim et al. [2023] have combined quantization with pruning and knowledge distillation in SqueezeLLM. Guan et al. [2024] have optimized the balance between compression and performance through mixed-precision quantization with APTQ. These developments significantly enhance the efficiency of LLMs.

Parameter Efficient Fine-Tuning. PEFT techniques have become crucial for enhancing LLMs without increasing inference overhead. Recent innovations have expanded the field. Dettmers et al. [2023] have introduced QLoRA, which combines 4-bit quantization with low-rank adapters. Li et al. [2023] have presented LoftQ, which alternates between quantization and low-rank approximation steps. Berman and Peherstorfer [2024] have introduced CoLoRA for accelerating the prediction of solution fields under new parameters. AdaLoRA Zhang et al. [2023a] proposes adaptive budget allocation for low-rank updates, while LQ-LoRA Guo et al. [2023] combines low-rank decomposition with quantization for efficient fine-tuning under memory constraints. Additionally, Zhou et al. [2024] have introduced RankAdaptor, which is a hierarchical dynamic low-rank adaptation method for structural pruned LLMs. These advancements offer innovative solutions for efficient LLM fine-tuning across diverse applications.

6 Conclusion

In this work, we propose QR-Adaptor, a unified, gradient-free method that uses partial calibration data to simultaneously optimize the precision and LoRA rank of each model layer. By focusing on the discrete nature of quantization and low-rank spaces and optimizing them within a task-driven framework, QR-Adaptor overcomes the limitations of iterative error-fitting techniques and rank-adaptive methods unsuitable for quantization. Our extensive experiments demonstrate that QR-Adaptor consistently outperforms existing baselines, achieving better performance than 16-bit fine-tuned models while maintaining a 4-bit memory footprint. These results highlight the importance of integrating quantization and low-rank matrices into a single, cohesive optimization process, driven by actual performance and memory efficiency.

References

- Jules Berman and Benjamin Peherstorfer. Colora: Continuous low-rank adaptation for reduced implicit neural modeling of parameterized partial differential equations, 2024. URL <https://arxiv.org/abs/2402.14646>.
- Yonatan Bisk, Rowan Zellers, Jianfeng Gao, Yejin Choi, et al. Piqa: Reasoning about physical commonsense in natural language. In *Proceedings of the AAAI conference on artificial intelligence*, volume 34, pages 7432–7439, 2020.
- Yupeng Chang, Xu Wang, Jindong Wang, Yuan Wu, Linyi Yang, Kaijie Zhu, Hao Chen, Xiaoyuan Yi, Cunxiang Wang, Yidong Wang, et al. A survey on evaluation of large language models. *ACM Transactions on Intelligent Systems and Technology*, 15(3):1–45, 2024.
- Christopher Clark, Kenton Lee, Ming-Wei Chang, Tom Kwiatkowski, Michael Collins, and Kristina Toutanova. Boolq: Exploring the surprising difficulty of natural yes/no questions. In *Proceedings of the 2019 Conference of the North American Chapter of the Association for Computational Linguistics: Human Language Technologies, Volume 1 (Long and Short Papers)*, pages 2924–2936, 2019.
- Peter Clark, Isaac Cowhey, Oren Etzioni, Tushar Khot, Ashish Sabharwal, Carissa Schoenick, and Oyvind Tafjord. Think you have solved question answering? try arc, the ai2 reasoning challenge. *arXiv preprint arXiv:1803.05457*, 2018.
- Kalyanmoy Deb, Amrit Pratap, Sameer Agarwal, and TAMT Meyarivan. A fast and elitist multiobjective genetic algorithm: Nsga-ii. *IEEE transactions on evolutionary computation*, 6(2):182–197, 2002.
- Tim Dettmers, Mike Lewis, Younes Belkada, and Luke Zettlemoyer. Llm.int8(): 8-bit matrix multiplication for transformers at scale. *CoRR*, abs/2208.07339, 2022. URL <http://arxiv.org/abs/2208.07339>.
- Tim Dettmers, Artidoro Pagnoni, Ari Holtzman, and Luke Zettlemoyer. Qlora: Efficient finetuning of quantized llms. *arXiv preprint arXiv:2305.14314*, 2023.
- Elias Frantar, Sahar Ashkboos, Torsten Hoefler, and Dan Alistarh. Gptq: Accurate post-training quantization for generative pre-trained transformers. In *The Eleventh International Conference on Learning Representations (ICLR)*, 2023.
- Yunchao Gong, Liu Liu, Ming Yang, and Lubomir Bourdev. Compressing deep convolutional networks using vector quantization. *arXiv preprint arXiv:1412.6115*, 2014.
- Zhuocheng Gong, Jiahao Liu, Jingang Wang, Xunliang Cai, Dongyan Zhao, and Rui Yan. What makes quantization for large language models hard? an empirical study from the lens of perturbation, 2024. URL <https://arxiv.org/abs/2403.06408>.
- Aaron Grattafiori, Abhimanyu Dubey, Abhinav Jauhri, Abhinav Pandey, Abhishek Kadian, Ahmad Al-Dahle, Aiesha Letman, Akhil Mathur, Alan Schelten, Alex Vaughan, Amy Yang, Angela Fan, Anirudh Goyal, Anthony Hartshorn, Aobo Yang, Archi Mitra, Archie Sravankumar, Artem Korenev, Arthur Hinsvark, Arun Rao, Aston Zhang, Aurelien Rodriguez, Austen Gregerson, Ava Spataru, Baptiste Roziere, Bethany Biron, Binh Tang, Bobbie Chern, Charlotte Caucheteux, Chaya Nayak, Chloe Bi, Chris Marra, Chris McConnell, Christian Keller, Christophe Touret, Chunyang Wu, Corinne Wong, Cristian Canton Ferrer, Cyrus Nikolaidis, Damien Allonsius, Daniel Song, Danielle Pintz, Danny Livshits, Danny Wyatt, David Esiobu, Dhruv Choudhary, Dhruv Mahajan, Diego Garcia-Olano, Diego Perino, Dieuwke Hupkes, Egor Lakomkin, Ehab AlBadawy, Elina Lobanova, Emily Dinan, Eric Michael Smith, Filip Radenovic, Francisco Guzmán, Frank Zhang, Gabriel Synnaeve, Gabrielle Lee, Georgia Lewis Anderson, Govind Thattai, Graeme Nail, Gregoire Mialon, Guan Pang, Guillem Cucurell, Hailey Nguyen, Hannah Korevaar, Hu Xu, Hugo Touvron, Iliyan Zarov, Imanol Arrieta Ibarra, Isabel Kloumann, Ishan Misra, Ivan Evtimov, Jack Zhang, Jade Copet, Jaewon Lee, Jan Geffert, Jana Vranes, Jason Park, Jay Mahadeokar, Jeet Shah, Jelfer van der Linde, Jennifer Billock, Jenny Hong, Jenya Lee, Jeremy Fu, Jianfeng Chi, Jianyu Huang, Jiawen Liu, Jie Wang, Jiecao Yu, Joanna Bitton, Joe Spisak, Jongsoo Park, Joseph Rocca, Joshua Johnstun, Joshua Saxe, Junteng Jia, Kalyan Vasuden Alwala, Karthik Prasad, Kartikeya Upasani, Kate Plawiak,

Ke Li, Kenneth Heafield, Kevin Stone, Khalid El-Arini, Krithika Iyer, Kshitiz Malik, Kuenley Chiu, Kunal Bhalla, Kushal Lakhotia, Lauren Rantala-Yearly, Laurens van der Maaten, Lawrence Chen, Liang Tan, Liz Jenkins, Louis Martin, Lovish Madaan, Lubo Malo, Lukas Blecher, Lukas Landzaat, Luke de Oliveira, Madeline Muzzi, Mahesh Pasupuleti, Mannat Singh, Manohar Paluri, Marcin Kardas, Maria Tsimpoukelli, Mathew Oldham, Mathieu Rita, Maya Pavlova, Melanie Kambadur, Mike Lewis, Min Si, Mitesh Kumar Singh, Mona Hassan, Naman Goyal, Narjes Torabi, Nikolay Bashlykov, Nikolay Bogoychev, Niladri Chatterji, Ning Zhang, Olivier Duchenne, Onur Çelebi, Patrick Alrassy, Pengchuan Zhang, Pengwei Li, Petar Vasic, Peter Weng, Prajjwal Bhargava, Pratik Dubal, Praveen Krishnan, Punit Singh Koura, Puxin Xu, Qing He, Qingxiao Dong, Ragavan Srinivasan, Raj Ganapathy, Ramon Calderer, Ricardo Silveira Cabral, Robert Stojnic, Roberta Raileanu, Rohan Maheswari, Rohit Girdhar, Rohit Patel, Romain Sauvestre, Ronnie Polidoro, Roshan Sumbaly, Ross Taylor, Ruan Silva, Rui Hou, Rui Wang, Saghar Hosseini, Sahana Chennabasappa, Sanjay Singh, Sean Bell, Seohyun Sonia Kim, Sergey Edunov, Shao-liang Nie, Sharan Narang, Sharath Rapparthi, Sheng Shen, Shengye Wan, Shruti Bhosale, Shun Zhang, Simon Vandenhende, Soumya Batra, Spencer Whitman, Sten Sootla, Stephane Collet, Suchin Gururangan, Sydney Borodinsky, Tamar Herman, Tara Fowler, Tarek Sheasha, Thomas Georgiou, Thomas Scialom, Tobias Speckbacher, Todor Mihaylov, Tong Xiao, Ujjwal Karn, Vedanuj Goswami, Vibhor Gupta, Vignesh Ramanathan, Viktor Kerkez, Vincent Gonguet, Virginie Do, Vish Vogeti, Vitor Albiero, Vladan Petrovic, Weiwei Chu, Wenhan Xiong, Wenyin Fu, Whitney Meers, Xavier Martinet, Xiaodong Wang, Xiaofang Wang, Xiaoqing Ellen Tan, Xide Xia, Xinfeng Xie, Xuchao Jia, Xuwei Wang, Yaelle Goldschlag, Yashesh Gaur, Yasmine Babaei, Yi Wen, Yiwen Song, Yuchen Zhang, Yue Li, Yuning Mao, Zacharie Delpierre Coudert, Zheng Yan, Zhengxing Chen, Zoe Papanikos, Aaditya Singh, Aayushi Srivastava, Abha Jain, Adam Kelsey, Adam Shajnfeld, Adithya Gangidi, Adolfo Victoria, Ahuva Goldstand, Ajay Menon, Ajay Sharma, Alex Boesenberg, Alexei Baevski, Allie Feinstein, Amanda Kallet, Amit Sangani, Amos Teo, Anam Yunus, Andrei Lupu, Andres Alvarado, Andrew Caples, Andrew Gu, Andrew Ho, Andrew Poulton, Andrew Ryan, Ankit Ramchandani, Annie Dong, Annie Franco, Anuj Goyal, Aparajita Saraf, Arkabandhu Chowdhury, Ashley Gabriel, Ashwin Bharambe, Assaf Eisenman, Azadeh Yazdan, Beau James, Ben Maurer, Benjamin Leonhardi, Bernie Huang, Beth Loyd, Beto De Paola, Bhargavi Paranjape, Bing Liu, Bo Wu, Boyu Ni, Braden Hancock, Bram Wasti, Brandon Spence, Brani Stojkovic, Brian Gamido, Britt Montalvo, Carl Parker, Carly Burton, Catalina Mejia, Ce Liu, Changhan Wang, Changkyu Kim, Chao Zhou, Chester Hu, Ching-Hsiang Chu, Chris Cai, Chris Tindal, Christoph Feichtenhofer, Cynthia Gao, Damon Civin, Dana Beaty, Daniel Kreymer, Daniel Li, David Adkins, David Xu, Davide Testuggine, Delia David, Devi Parikh, Diana Liskovich, Didem Foss, Dingkan Wang, Duc Le, Dustin Holland, Edward Dowling, Eissa Jamil, Elaine Montgomery, Eleonora Presani, Emily Hahn, Emily Wood, Eric-Tuan Le, Erik Brinkman, Esteban Arcaute, Evan Dunbar, Evan Smothers, Fei Sun, Felix Kreuk, Feng Tian, Filippos Kokkinos, Firat Ozgenel, Francesco Caggioni, Frank Kanayet, Frank Seide, Gabriela Medina Florez, Gabriella Schwarz, Gada Badeer, Georgia Swee, Gil Halpern, Grant Herman, Grigory Sizov, Guangyi, Zhang, Guna Lakshminarayanan, Hakan Inan, Hamid Shojanazeri, Han Zou, Hannah Wang, Hanwen Zha, Haroun Habeeb, Harrison Rudolph, Helen Suk, Henry Aspegren, Hunter Goldman, Hongyuan Zhan, Ibrahim Damlaj, Igor Molybog, Igor Tufanov, Ilias Leontiadis, Irina-Elena Veliche, Itai Gat, Jake Weissman, James Geboski, James Kohli, Janice Lam, Japhet Asher, Jean-Baptiste Gaya, Jeff Marcus, Jeff Tang, Jennifer Chan, Jenny Zhen, Jeremy Reizenstein, Jeremy Teboul, Jessica Zhong, Jian Jin, Jingyi Yang, Joe Cummings, Jon Carvill, Jon Shepard, Jonathan McPhie, Jonathan Torres, Josh Ginsburg, Junjie Wang, Kai Wu, Kam Hou U, Karan Saxena, Kartikay Khandelwal, Katayoun Zand, Kathy Matosich, Kaushik Veeraraghavan, Kelly Michelena, Keqian Li, Kiran Jagadeesh, Kun Huang, Kunal Chawla, Kyle Huang, Lailin Chen, Lakshya Garg, Lavender A, Leandro Silva, Lee Bell, Lei Zhang, Liangpeng Guo, Licheng Yu, Liron Moshkovich, Luca Wehrstedt, Madian Khabsa, Manav Avalani, Manish Bhatt, Martynas Mankus, Matan Hasson, Matthew Lennie, Matthias Reso, Maxim Groshev, Maxim Naumov, Maya Lathi, Meghan Keneally, Miao Liu, Michael L. Seltzer, Michal Valko, Michelle Restrepo, Mihir Patel, Mik Vyatskov, Mikayel Samvelyan, Mike Clark, Mike Macey, Mike Wang, Miquel Juber Hermoso, Mo Metanat, Mohammad Rastegari, Munish Bansal, Nandhini Santhanam, Natascha Parks, Natasha White, Navyata Bawa, Nayan Singhal, Nick Egebo, Nicolas Usunier, Nikhil Mehta, Nikolay Pavlovich Laptev, Ning Dong, Norman Cheng, Oleg Chernoguz, Olivia Hart, Omkar Salpekar, Ozlem Kalinli, Parkin Kent, Parth Parekh, Paul Saab, Pavan Balaji, Pedro Rittner, Philip Bontrager, Pierre Roux, Piotr Dollar, Polina Zvyagina, Prashant Ratanchandani, Pritish Yuvraj, Qian Liang, Rachad Alao, Rachel Rodriguez, Rafi Ayub, Raghotham Murthy, Raghu Nayani, Rahul Mitra, Rangaprabhu Parthasarathy, Raymond Li, Rebekkah Hogan, Robin

- Batthey, Rocky Wang, Russ Howes, Ruty Rinott, Sachin Mehta, Sachin Siby, Sai Jayesh Bondu, Samyak Datta, Sara Chugh, Sara Hunt, Sargun Dhillon, Sasha Sidorov, Satadru Pan, Saurabh Mahajan, Saurabh Verma, Seiji Yamamoto, Sharadh Ramaswamy, Shaun Lindsay, Sheng Feng, Shenghao Lin, Shengxin Cindy Zha, Shishir Patil, Shiva Shankar, Shuqiang Zhang, Shuqiang Zhang, Sinong Wang, Sneha Agarwal, Soji Sajuyigbe, Soumith Chintala, Stephanie Max, Stephen Chen, Steve Kehoe, Steve Satterfield, Sudarshan Govindaprasad, Sumit Gupta, Summer Deng, Sungmin Cho, Sunny Virk, Suraj Subramanian, Sy Choudhury, Sydney Goldman, Tal Remez, Tamar Glaser, Tamara Best, Thilo Koehler, Thomas Robinson, Tianhe Li, Tianjun Zhang, Tim Matthews, Timothy Chou, Tzook Shaked, Varun Vontimitta, Victoria Ajayi, Victoria Montanez, Vijai Mohan, Vinay Satish Kumar, Vishal Mangla, Vlad Ionescu, Vlad Poenaru, Vlad Tiberiu Mihailescu, Vladimir Ivanov, Wei Li, Wenchen Wang, Wenwen Jiang, Wes Bouaziz, Will Constable, Xiaocheng Tang, Xiaojian Wu, Xiaolan Wang, Xilun Wu, Xinbo Gao, Yaniv Kleinman, Yanjun Chen, Ye Hu, Ye Jia, Ye Qi, Yenda Li, Yilin Zhang, Ying Zhang, Yossi Adi, Youngjin Nam, Yu, Wang, Yu Zhao, Yuchen Hao, Yundi Qian, Yunlu Li, Yuzi He, Zach Rait, Zachary DeVito, Zef Rosnbrick, Zhaoduo Wen, Zhenyu Yang, Zhiwei Zhao, and Zhiyu Ma. The llama 3 herd of models, 2024. URL <https://arxiv.org/abs/2407.21783>.
- Zhaoyi Guan, Hongyi Huang, Yihan Su, Haoxiang Huang, Ngai Wong, and Huazhong Yu. Aptq: Attention-aware post-training mixed-precision quantization for large language models. *arXiv preprint arXiv:2402.14866*, 2024.
- Han Guo, Philip Greengard, Eric Xing, and Yoon Kim. Lq-lora: Low-rank plus quantized matrix decomposition for efficient language model finetuning. *ICLR 2024*, 2023.
- Han Guo, Philip Greengard, Eric Xing, and Yoon Kim. LQ-loRA: Low-rank plus quantized matrix decomposition for efficient language model finetuning. In *The Twelfth International Conference on Learning Representations*, 2024. URL <https://openreview.net/forum?id=xw29VvOMmU>.
- Suyog Gupta, Ankur Agrawal, Kailash Gopalakrishnan, and Pritish Narayanan. Deep learning with limited numerical precision. In *International conference on machine learning*, pages 1737–1746. PMLR, 2015.
- Dan Hendrycks, Collin Burns, Steven Basart, Andy Zou, Mantas Mazeika, Dawn Song, and Jacob Steinhardt. Measuring massive multitask language understanding. In *International Conference on Learning Representations*, 2021. URL <https://openreview.net/forum?id=d7KBjmI3GmQ>.
- Edward J. Hu, Yelong Shen, Phillip Wallis, Zeyuan Allen-Zhu, Yuanzhi Li, Shean Wang, Lu Wang, and Weizhu Chen. Lora: Low-rank adaptation of large language models. In *Proceedings of ICLR*, 2022.
- Sehoon Kim, Connor R. C. Hooper, Amir Gholami, Zhen Dong, Xiuyu Li, Sheng Shen, and Kurt Keutzer. Squeezellm: Dense-and-sparse quantization. In *Proceedings of the Forty-first International Conference on Machine Learning (ICML)*, 2023.
- Yixiao Li, Yifan Yu, Chen Liang, Pengcheng He, Nikos Karampatziakis, Weizhu Chen, and Tuo Zhao. Loftq: Lora-fine-tuning-aware quantization for large language models, 2023. URL <https://arxiv.org/abs/2310.08659>.
- Ji Lin, Jie Tang, Haotao Tang, Shuxin Yang, Xiaoxia Dang, and Song Han. Awq: Activation-aware weight quantization for llm compression and acceleration. *arXiv preprint arXiv:2306.00978*, 2023.
- Spyros Makridakis, Fotios Petropoulos, and Yanfei Kang. Large language models: Their success and impact. *Forecasting*, 5(3):536–549, 2023.
- Todor Mihaylov, Peter Clark, Tushar Khot, and Ashish Sabharwal. Can a suit of armor conduct electricity? a new dataset for open book question answering. In *Proceedings of the 2018 Conference on Empirical Methods in Natural Language Processing*, pages 2381–2391, 2018.
- Mohaimenul Azam Khan Raiaan, Md Saddam Hossain Mukta, Kaniz Fatema, Nur Mohammad Fahad, Sadman Sakib, Most Marufatul Jannat Mim, Jubaer Ahmad, Mohammed Eunus Ali, and Sami Azam. A review on large language models: Architectures, applications, taxonomies, open issues and challenges. *IEEE Access*, 2024.

- Keisuke Sakaguchi, Ronan Le Bras, Chandra Bhagavatula, and Yejin Choi. Winogrande: An adversarial winograd schema challenge at scale. *Communications of the ACM*, 64(9):99–106, 2021.
- Rohan Taori, Ishaan Gulrajani, Tianyi Zhang, Yann Dubois, Xuechen Li, Carlos Guestrin, Percy Liang, and Tatsunori B. Hashimoto. Stanford alpaca: An instruction-following llama model. *Stanford CRFM*, 2023. URL https://github.com/tatsu-lab/stanford_alpaca.
- Hugo Touvron, Louis Martin, Kevin Stone, Peter Albert, Amjad Almahairi, Yasmine Babaei, Nikolay Bashlykov, Soumya Batra, Prajjwal Bhargava, and et al. Bhosale, Shruti. Llama 2: Open foundation and fine-tuned chat models. *arXiv preprint arXiv:2307.09288*, 2023.
- Zhongwei Wan, Xin Wang, Che Liu, Samiul Alam, Yu Zheng, Jiachen Liu, Zhongnan Qu, Shen Yan, Yi Zhu, Quanlu Zhang, et al. Efficient large language models: A survey. *Transactions on Machine Learning Research*, 2023.
- Zhewei Yao, Reza Yazdani Aminabadi, Ming Zhang, Xiang Wu, Cong Li, and Yuxiong He. Zeroquant: Efficient and affordable post-training quantization for large-scale transformers. In *Advances in Neural Information Processing Systems*, volume 35, pages 27168–27183, 2022.
- Rowan Zellers, Ari Holtzman, Yonatan Bisk, Ali Farhadi, and Yejin Choi. Hellaswag: Can a machine really finish your sentence? In *Proceedings of the 57th Annual Meeting of the Association for Computational Linguistics*, pages 4791–4800, 2019.
- Qingru Zhang, Minshuo Chen, Alexander Bukharin, Pengcheng He, Yu Cheng, Weizhu Chen, and Tuo Zhao. Adaptive budget allocation for parameter-efficient fine-tuning. In *International Conference on Learning Representations*. Openreview, 2023a.
- Qingru Zhang, Minshuo Chen, Alexander Bukharin, Nikos Karampatziakis, Pengcheng He, Yu Cheng, Weizhu Chen, and Tuo Zhao. Adalora: Adaptive budget allocation for parameter-efficient fine-tuning. *arXiv preprint arXiv:2303.10512*, 2023b.
- Changhai Zhou, Shijie Han, Shiyang Zhang, Shichao Weng, Zekai Liu, and Cheng Jin. Rankadaptor: Hierarchical dynamic low-rank adaptation for structural pruned llms. *arXiv preprint arXiv:2406.15734*, 2024.

A Trajectories

To compare the training trajectories of the full-precision model, the standard quantized model, and LoFTQ with varying numbers of iterations, we periodically saved “parameter snapshots” from each model during fine-tuning. Specifically, at every 50 training steps, we extracted all trainable weights—including the LoRA/Adapter A/B matrices for LoFTQ—and saved them to disk, yielding around 10–20 snapshots per model. We then concatenated these snapshots into a $[3T, D]$ parameter matrix (where T is the number of snapshots per model and D is the dimension of the flattened parameter vectors). Next, we applied Principal Component Analysis (PCA) using scikit-learn’s PCA module to learn a 2D projection across all snapshots. For visualization, each model’s snapshots were transformed into the resulting 2D space and plotted in Matplotlib, with the points connected in chronological order to depict the evolution of parameters during training. In the figure, blue circles represent the trajectory of the original full-precision (FP32) model, orange triangles correspond to the fully quantized model, and green squares, red diamonds, and purple crosses indicate LoFTQ after 1, 5, and 10 iterations, respectively. From this 2D PCA projection, we observe that LoFTQ-1 remains relatively close to the FP32 path, suggesting that even a single iteration of LoFTQ helps narrow the performance gap. However, increasing the number of LoFTQ iterations does not continuously improve convergence: LoFTQ-5 and especially LoFTQ-10 deviate more substantially from both FP32 and fully quantized trajectories, with LoFTQ-10 extending abnormally far along the PCA axes. These findings suggest that while LoFTQ offers an initial boost by moving closer to the uncompressed model, additional iterations may lead the optimization path away from more optimal parameter regions, limiting further gains in performance.

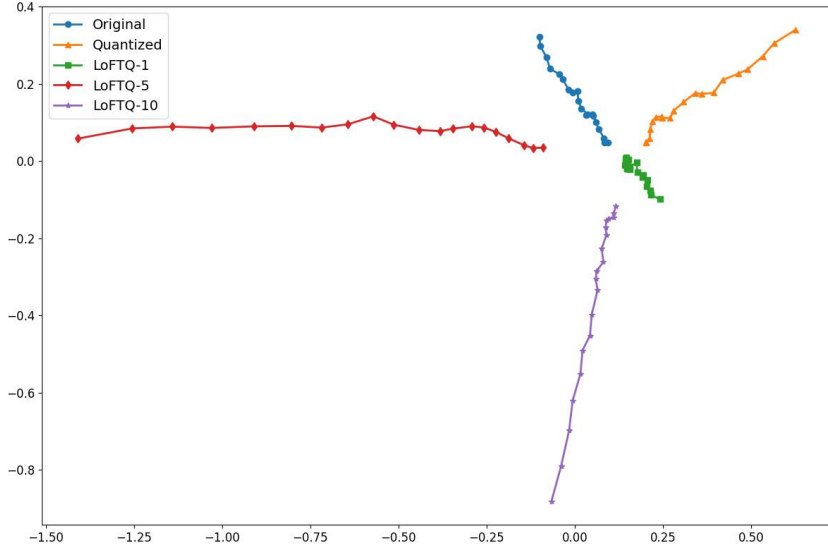


Figure 5: 2D PCA projection of parameter trajectories from three models during fine-tuning. We saved weight snapshots at regular intervals, concatenated them into a $[3T, D]$ matrix, and used PCA to reduce the dimensionality to two. The blue curve (circles) represents the original full-precision model, the orange curve (triangles) denotes the standard quantized model, and the green squares, red diamonds, and purple crosses correspond to LoFTQ after 1, 5, and 10 iterations, respectively. While LoFTQ-1 stays relatively close to the FP32 path, additional LoFTQ iterations do not sustain that initial convergence advantage, as LoFTQ-5 and LoFTQ-10 deviate more significantly and form longer, more anomalous trajectories in the PCA space.

B quantization

We first apply NF-quantization with bit size b_0 and bucket size B_0 to obtain the quantized matrix \widehat{A}_i and the absmax values for each block $s = [s_1, \dots, s_{\text{sizeof}(A_i)}]$. These absmax values are further quantized to b_1 bits via uniform integer quantization with bucket size B_1 to obtain the quantized

vector \hat{s} , along with the absmax values for s , i.e., $v = [v_1, \dots, v_{\frac{\text{sizeof}(A_i)}{B_0 B_1}}]$. Finally, we cast v to b_2 bits to obtain \hat{v} .

This quantization scheme requires storing $\hat{A}_i, \hat{s}, \hat{v}$ to represent A_i . We can thus quantify the memory cost (number of bits) for storing A_i given a configuration $c_i = (b_0, b_1, b_2, B_0, B_1)$ as:

$$\text{memory_cost}(A_i, c_i) = \text{sizeof}(A_i) \cdot \left(b_0 + \frac{b_1}{B_0} + \frac{b_2}{B_0 \cdot B_1} \right) \quad (16)$$

The original NF-4 double quantization is a special case with $q_{\text{NF4}} = (4, 8, \text{fp32}, 64, 256)$ and $\text{memory_cost}(A_i, q_{\text{NF4}}) = 4.127 \cdot \text{sizeof}(A_i)$, i.e., NF-4 requires on average 4.127 bits per parameter.

C Pseudo code of the specific algorithm in the QR-Adaptor framework

Due to page limitations, we present the pseudocode of the algorithm in Section 3 below.

Algorithm 1 Pareto Rank Calculation

- 1: **Input:** Population P with n individuals
 - 2: Calculate the number of dominated individuals n_p and the set of solutions dominated S_p for each individual p
 - 3: Place individuals with $n_p = 0$ into set F_1
 - 4: **for** each individual i in F_1 **do**
 - 5: **for** each individual $j \in S_i$ **do**
 - 6: $n_j \leftarrow n_j - 1$
 - 7: **if** $n_j = 0$ **then**
 - 8: Add individual j to set F_2
 - 9: **end if**
 - 10: **end for**
 - 11: **end for**
 - 12: Repeat for F_2, F_3, \dots , until all individuals are ranked
 - 13: **Output:** Pareto-ranked individuals
-

Algorithm 3 Simulated Binary Crossover (SBX)

- Require:** Two parent individuals P_1 and P_2 , each with L real-valued genes
- 1: Initialize offspring O_1 and O_2 as empty
 - 2: **for** $l = 1$ to L **do**
 - 3: Generate a random number $u \in [0, 1]$
 - 4: **if** $u \leq 0.5$ **then**
 - 5: $\beta \leftarrow (2u)^{1/(n+1)}$
 - 6: **else**
 - 7: $\beta \leftarrow \left(\frac{1}{2(1-u)} \right)^{1/(n+1)}$
 - 8: **end if**
 - 9: $y_{1l} \leftarrow 0.5 \cdot ((1 + \beta) \cdot p_{1l} + (1 - \beta) \cdot p_{2l})$
 - 10: $y_{2l} \leftarrow 0.5 \cdot ((1 - \beta) \cdot p_{1l} + (1 + \beta) \cdot p_{2l})$
 - 11: Append y_{1l} to O_1 and y_{2l} to O_2
 - 12: **end for**
 - 13: **Output:** O_1 and O_2
-

Algorithm 2 Crowding Distance Calculation

- 1: **Input:** Ranked individuals F with N individuals, M objectives
 - 2: **for** each individual $n \in 1 \dots N$ **do**
 - 3: Initialize $d_n \leftarrow 0$
 - 4: **end for**
 - 5: **for** each objective function f_m **do**
 - 6: Sort individuals based on f_m
 - 7: $f_m^{\max}, f_m^{\min} \leftarrow \max f_m, \min f_m$
 - 8: $d_1, d_N \leftarrow \infty$
 - 9: **for** $n = 2$ to $N - 1$ **do**
 - 10: $d_n \leftarrow d_n + \frac{f_m(n+1) - f_m(n-1)}{f_m^{\max} - f_m^{\min}}$
 - 11: **end for**
 - 12: **end for**
 - 13: **Output:** Crowding distances d_n for each individual n
-

Algorithm 4 Polynomial Mutation

- Require:** Individual P with L real-valued genes, mutation probability p_m
- 1: Initialize mutated individual P' as a copy of P
 - 2: **for** $l = 1$ to L **do**
 - 3: Generate a random number $u \in [0, 1]$
 - 4: **if** $u < p_m$ **then**
 - 5: Generate a random number $\delta \in [-1, 1]$
 - 6: $x'_l \leftarrow x_l + (x_{\max} - x_{\min}) \cdot \delta \cdot (1 - |\delta|)^{n-1}$
 - 7: Replace x_l with x'_l in P'
 - 8: **end if**
 - 9: **end for**
 - 10: **Output:** Mutated individual P'
-

Table 2: Performance comparison of different methods across various bit-width configurations on Llama2-7B. Superscripts on LoftQ bits indicate the number of initialization iterations. QR-Adaptor searches for optimal bit number and rank value for each layer based on different tasks with its bit number averaged across tasks. Bold figures represent the best performance for a given model and task, while underlined figures indicate the second-best. Accuracy is reported as %.

	Method	Bit	ARC(C)	ARC(E)	BoolQ	HellaS	OBQA	PIQA	WinoG	Average
Rank = 8	LoRA	16	46.93	<u>77.36</u>	<u>78.47</u>	76.93	44.80	79.38	69.38	67.61
	QLoRA	8	48.21	<u>77.36</u>	77.92	<u>76.88</u>	44.80	<u>79.82</u>	68.75	<u>67.70</u>
	QLoRA	4	46.25	76.26	77.43	76.42	46.20	78.67	<u>69.85</u>	67.30
	AdaLoRA	16	46.08	76.77	77.46	75.89	44.20	79.16	69.22	66.97
	AdaLoRA	8	46.08	76.73	77.49	75.93	44.20	79.00	69.06	66.93
	AdaLoRA	4	46.33	75.25	76.39	75.45	44.40	77.91	69.14	66.41
	LoftQ	4 ¹	46.16	77.10	77.43	76.68	44.80	79.33	69.30	67.26
	LoftQ	4 ⁵	47.35	76.64	76.33	76.36	45.60	79.05	69.06	67.20
	LQ-LoRA	4	47.18	76.60	76.54	76.24	45.00	78.84	68.90	67.04
	QR-Adaptor	5.45	<u>48.04</u>	77.44	78.96	<u>76.84</u>	<u>46.00</u>	79.86	69.97	68.15
Rank = 16	LoRA	16	46.93	77.57	<u>78.41</u>	76.81	45.00	79.38	69.06	67.59
	QLoRA	8	47.61	<u>77.44</u>	<u>78.41</u>	76.93	45.40	79.05	69.06	67.70
	QLoRA	4	46.67	<u>76.35</u>	77.25	76.40	45.00	78.84	<u>70.01</u>	67.22
	AdaLoRA	16	46.16	76.68	77.58	75.92	44.20	79.11	69.38	67.00
	AdaLoRA	8	46.16	76.68	77.40	75.91	44.40	79.11	69.06	66.96
	AdaLoRA	4	46.33	75.29	76.45	75.44	44.20	77.91	69.46	66.47
	LoftQ	4 ¹	47.10	77.19	77.89	76.61	44.80	<u>79.43</u>	69.69	67.53
	LoftQ	4 ⁵	<u>47.95</u>	76.47	76.79	76.25	45.60	78.51	69.61	67.31
	LQ-LoRA	4	47.10	76.39	77.22	76.33	46.40	78.78	70.09	67.47
	QR-Adaptor	5.45	48.04	<u>77.44</u>	78.96	<u>76.84</u>	<u>46.00</u>	79.86	69.97	68.15

D More Results

Due to page limitations, we present remaining results across various models here.

D.1 Experiment Scope Expansion: Llama 2 Series

In the original experiments, the focus was primarily on Llama3.1, considering that its updated architecture present new challenges for quantization. Compared to Llama2 series, Llama3.1 is significantly harder to quantize, especially under low-bit configurations, as they incorporate more sophisticated architectural features. Additionally, to comprehensively demonstrate the superiority of **QR-Adaptor**, we have also conducted extensive performance experiments on the Llama2 series models, with the results presented in Table 2 and Table 3.

Our results show that **QR-Adaptor** consistently demonstrates superior performance across all tasks and outperforms existing methods, such as AdaLoRA and LoftQ, on Llama 2 series. The robustness of **QR-Adaptor** is also evident, especially on tasks that typically cause performance degradation for other methods.

D.2 Visualization Results for the MMLU Task

The results for the MMLU task in LLaMA2 are shown in Figure 6. **QR-Adaptor** demonstrates outstanding performance across various benchmarks. Due to the rank value selection ranging from 2 to 16, in some cases, **QR-Adaptor** consumes less memory than the fine-tuned 4-bit quantized models. Moreover, the low-precision models fine-tuned by **QR-Adaptor** outperform the fine-tuned 16-bit models. Another advantage of the **QR-Adaptor** is that it can be implemented without any additional technical measures to optimize performance, apart from spending some time (about 15 minutes to get one data point). This simple but effective method is very useful in practical applications.

Table 3: Performance comparison of different methods across various bit-width configurations on Llama2-13B. Superscripts on LoftQ bits indicate the number of initialization iterations. QR-Adaptor searches for optimal bit number and rank value for each layer based on different tasks with its bit number averaged across tasks. Bold figures represent the best performance for a given model and task, while underlined figures indicate the second-best. Accuracy is reported as %.

	Method	Bit	ARC(C)	ARC(E)	BoolQ	HellaS	OBQA	PIQA	WinoG	Average
Rank = 8	LoRA	16	<u>52.56</u>	<u>80.18</u>	81.44	79.98	46.40	<u>81.12</u>	71.98	<u>70.52</u>
	QLoRA	8	52.39	<u>80.18</u>	81.22	79.92	45.00	80.47	73.09	70.32
	QLoRA	4	51.54	78.91	81.41	79.46	45.40	80.30	71.82	69.83
	AdaLoRA	16	49.15	79.46	80.37	79.25	45.40	80.47	72.30	69.49
	AdaLoRA	8	49.32	79.34	80.43	79.29	45.60	80.47	72.22	69.52
	AdaLoRA	4	48.29	77.78	80.40	78.12	44.20	80.14	71.74	68.67
	LoftQ	4 ¹	50.68	78.79	81.16	79.12	<u>45.80</u>	80.41	71.35	69.62
	LoftQ	4 ⁵	50.34	78.87	80.24	78.81	45.20	80.25	70.80	69.22
	LQ-LoRA	4	50.60	78.79	80.67	78.91	45.00	80.14	71.11	69.32
	QR-Adaptor	6.125	52.82	80.64	81.84	80.08	<u>45.80</u>	81.45	<u>72.69</u>	70.76
Rank = 16	LoRA	16	<u>52.13</u>	79.84	<u>81.50</u>	<u>80.07</u>	46.20	<u>81.23</u>	71.98	<u>70.42</u>
	QLoRA	8	51.54	<u>80.01</u>	81.13	79.86	46.20	81.18	72.22	70.31
	QLoRA	4	51.45	79.04	81.04	79.48	45.60	80.47	71.82	69.84
	AdaLoRA	16	49.40	79.34	80.46	79.28	45.40	80.47	72.30	69.52
	AdaLoRA	8	49.49	79.29	80.40	79.27	45.40	<u>80.52</u>	<u>72.38</u>	69.54
	AdaLoRA	4	48.29	77.69	80.43	78.10	44.20	80.09	71.67	68.64
	LoftQ	4 ¹	50.68	78.87	80.86	79.18	<u>45.80</u>	80.30	71.90	69.66
	LoftQ	4 ⁵	50.60	78.96	80.92	79.15	45.40	80.41	71.59	69.58
	LQ-LoRA	4	50.09	78.79	80.43	79.06	45.40	80.14	71.67	69.37
	QR-Adaptor	6.125	52.82	80.64	81.84	80.08	<u>45.80</u>	81.45	<u>72.69</u>	70.76

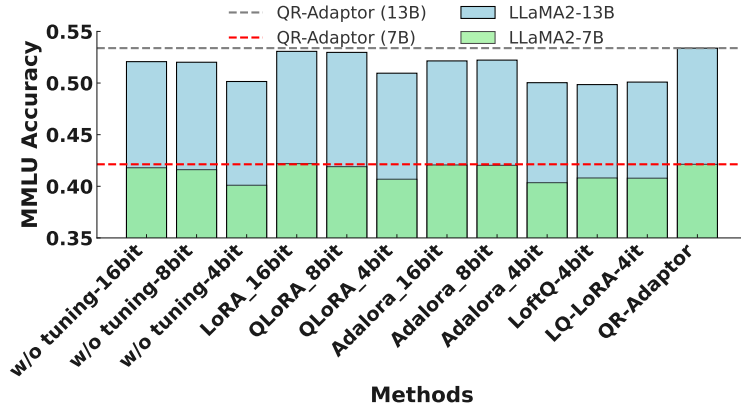


Figure 6: Performance comparison on MMLU benchmark. QR-Adaptor outperforms other methods.

D.3 Effectiveness on Larger Datasets with Higher Ranks

To address the concern regarding the effectiveness of small LoRA ranks on larger datasets, we conducted additional experiments on the LLaMA3.1-8B model using a larger dataset consisting of 177k samples. We tested our method with higher LoRA ranks (32 and 64) to evaluate its performance in handling large-scale data.

Our results are summarized in Table 4. The table compares the performance of **QR-Adaptor** with other baseline methods, including LoRA, QLoRA, AdaLoRA, and LoftQ, across various tasks. The performance metrics include accuracy scores on datasets such as ARC (Challenge), ARC (Easy), BoolQ, HellaSwag, OpenBookQA, PIQA, WinoGrande, and MMLU.

Table 4: Performance comparison of different methods across various bit-width configurations on Llama3.1-8B with higher ranks. Superscripts on LoftQ bits indicate the number of initialization iterations. QR-Adaptor searches for optimal bit number and rank value for each layer based on different tasks with its bit number averaged across tasks. Bold figures represent the best performance for a given model and task, while underlined figures indicate the second-best. Accuracy is reported as %.

Method	Rank	Bit	ARC(C)	ARC(E)	BoolQ	HellaS	OBQA	PIQA	WinoG	MMLU	Average
LoRA	32	16	54.86	82.74	82.75	<u>79.21</u>	44.40	<u>81.99</u>	74.11	63.66	70.47
LoRA	64	16	<u>55.46</u>	82.95	<u>82.94</u>	<u>79.13</u>	45.00	81.88	<u>74.51</u>	<u>64.34</u>	<u>70.78</u>
QLoRA	32	8	55.20	<u>83.12</u>	81.93	79.07	46.20	81.88	73.32	63.28	70.50
QLoRA	32	4	53.41	80.89	82.05	78.42	43.60	80.90	73.01	60.97	69.16
QLoRA	64	8	<u>55.46</u>	83.04	81.96	79.17	<u>45.80</u>	81.94	73.01	63.34	70.47
QLoRA	64	4	53.41	81.19	81.74	78.35	44.60	80.69	72.06	60.79	69.10
AdaLoRA	32	8	53.92	81.82	82.20	78.57	46.20	81.50	73.40	63.82	70.18
AdaLoRA	32	4	51.45	81.02	80.86	77.30	42.40	80.96	72.53	58.15	68.08
AdaLoRA	64	8	53.92	82.11	81.93	78.74	46.20	81.39	73.95	63.88	70.27
AdaLoRA	64	4	52.13	80.98	81.04	77.20	42.20	80.85	72.77	58.07	68.16
LoftQ	32	4 ¹	53.84	81.36	81.41	78.12	43.00	81.50	73.56	59.40	69.02
LoftQ	32	4 ⁵	52.56	81.36	81.96	78.05	42.80	81.45	73.09	59.41	68.84
LoftQ	32	4 ¹⁰	51.62	81.31	82.51	78.16	43.60	81.34	72.30	59.12	68.75
LoftQ	64	4 ¹	52.82	81.40	81.59	78.23	43.20	81.34	73.88	59.78	69.03
LoftQ	64	4 ⁵	52.39	81.10	81.13	78.33	43.40	81.34	73.24	58.69	68.70
LoftQ	64	4 ¹⁰	51.71	81.23	81.62	78.37	43.20	81.01	72.77	59.25	68.65
QR-Adaptor	32	5.875	56.12	83.45	83.21	79.78	46.20	82.10	74.59	64.40	71.23

Key Observations

- **Effectiveness of LoRA Initialization:** Despite using higher ranks (32 and 64) and larger datasets, methods like LoftQ and LQ-LoRA do not consistently outperform the standard QLoRA baseline or the quantized models without fine-tuning. Increasing iterations in LoftQ (from LoftQ-1 to LoftQ-10) to better fit quantization errors leads to performance degradation, especially on challenging tasks like MMLU and GSM8K. These results suggest that fitting quantization errors using LoRA initialization is not universally effective and may introduce noise that hinders model performance.
- **Effectiveness on Larger Datasets:** Our method, **QR-Adaptor**, consistently achieves superior performance across all tasks and outperforms other methods, confirming its robustness and scalability. The results validate that **QR-Adaptor** is effective even when small LoRA ranks might not suffice for larger datasets.
- **Impact of Adaptive LoRA Rank Reduction:** AdaLoRA exhibits performance drops, particularly with lower bit-widths and on more challenging tasks. This supports our observation that dynamically adjusting the rank during fine-tuning can lead to convergence issues in quantized models, which are less robust due to quantization errors.

These results reinforce our initial observations and highlight the limitations of methods that attempt to fit quantization errors through LoRA initialization. The inability of LoftQ and AdaLoRA to improve performance significantly, even with higher ranks and larger datasets, underscores the challenges associated with such approaches. In contrast, **QR-Adaptor**, guided by our proposed constraints, demonstrates consistent performance improvements.

D.4 Training Time Comparison

An important consideration in the evaluation of QR-Adaptor is the training time, particularly due to its reliance on Bayesian optimization. While QR-Adaptor provides significant performance improvements, it may require additional time per iteration compared to other methods. Table 5 summarizes the training time per iteration for QR-Adaptor and baseline methods on Llama2-7B.

Although QR-Adaptor takes longer to train due to its optimization process, this trade-off results in superior performance, particularly in terms of task-specific optimizations. The Bayesian optimization employed by QR-Adaptor ensures more precise adjustments to the model, which leads to better results on downstream tasks without additional resource consumption during the optimization process.

Table 5: Training time per iteration for different methods on Llama2-7B.

Method	Time per Iteration (min)
LoftQ	9
QR-Adaptor	15

D.5 Fairer Comparison: Matching Bit-width Configurations

Another important consideration for a fair comparison of quantization methods is the bit-width configuration used. To ensure that prior methods are evaluated under the same conditions as QR-Adaptor, we have re-evaluated AdaLoRA and LoftQ using the same mixed-precision configurations that were optimized through QR-Adaptor’s framework. The updated results for Llama 2-13B are shown in Table 6.

Table 6: Performance comparison with fair bit-width configurations for Llama2-13B. Accuracy is reported as %

Method	BoolQ	PIQA	HellaS	WinoG	ARC(E)	ARC(C)	OBQA	Average
AdaLoRA	81.08	80.13	79.21	71.74	79.51	50.12	45.60	69.77
LoftQ	80.93	79.47	79.02	71.34	79.26	51.20	45.60	69.98
QR-Adaptor	81.84	81.45	80.08	72.69	80.64	52.82	45.80	70.76

The results indicate that the initialization constraints applied by QR-Adaptor provide substantial improvements over the original configurations of AdaLoRA and LoftQ. Despite these improvements, QR-Adaptor still outperforms these methods in terms of overall task performance. The constraints, specifically ensuring stable initialization and fixing trainable parameters, contribute significantly to the enhanced performance of QR-Adaptor.

D.6 Impact of Longer Fine-tuning Epochs on Unfixed Parameters

While increasing the fine-tuning epochs for AdaLoRA can lead to some performance improvements, these gains are marginal and AdaLoRA still does not outperform other methods like LoRA, QLoRA, or our proposed QR-Adaptor.

Findings

- **Marginal Improvement with Increased Epochs:** Extending the training of AdaLoRA from 2 epochs to 5 epochs results in a slight performance increase. However, this improvement is not substantial and comes at the cost of significantly longer training times.
- **Need for Mixed-Precision with Adaptive Rank:** The results suggest that adaptive rank adjustment alone, as in AdaLoRA, may not be the most effective approach. The combination of adaptive rank with mixed-precision quantization, as in QR-Adaptor, yields superior performance.

Supporting Data

We provide an updated table below that includes an "Epochs" column, showing the results for LoRA, QLoRA, AdaLoRA (at 2 and 5 epochs), and QR-Adaptor.

Observation

- **AdaLoRA’s Performance with Increased Epochs:** As observed, AdaLoRA shows only slight performance improvements when training is extended from 2 to 5 epochs. Even with

Table 7: Performance comparison of different methods with varying fine-tuning epochs on Llama3.1-8B. Accuracy is reported as %

Method	Rank	Bit-width	Epochs	ARC (C)	ARC (E)	BoolQ	GSM8K (S)	GSM8K (F)	HellaS	OBQA	PIQA	WinoG
LoRA	8	16	2	56.14	83.88	83.18	54.36	54.28	79.44	45.20	82.10	75.30
QLoRA	8	8	2	57.08	83.46	82.48	53.75	53.90	79.63	46.00	82.10	74.59
QLoRA	8	4	2	54.35	82.41	82.08	44.35	44.50	78.82	44.20	81.50	73.64
AdaLoRA	8	16	2	52.90	81.99	81.87	50.57	50.57	78.65	45.00	81.34	73.95
AdaLoRA	8	16	5	53.50	82.25	82.05	51.00	50.90	78.75	45.20	81.40	74.10
AdaLoRA	8	8	2	52.90	81.86	82.05	49.96	49.96	78.65	44.80	81.34	74.43
AdaLoRA	8	8	5	53.10	82.00	82.10	50.20	50.10	78.70	45.20	81.38	74.50
AdaLoRA	8	4	2	51.28	80.98	80.61	37.83	38.36	77.36	42.80	80.74	72.53
AdaLoRA	8	4	5	51.50	81.10	80.75	38.00	38.50	77.40	43.20	80.78	72.60
QR-Adaptor	8	5.375	2	56.83	84.12	83.38	56.29	56.11	80.93	45.80	82.92	75.10

the increase in epochs, AdaLoRA’s performance does not surpass that of LoRA, QLoRA, or QR-Adaptor at 2 epochs.

- **QR-Adaptor’s Consistency:** QR-Adaptor consistently achieves superior performance across all tasks, further validating the effectiveness of our method over other adaptive rank-based approaches.
- **16-bit AdaLoRA Performance:** Notably, AdaLoRA with 16-bit precision (not quantized) still underperforms compared to LoRA and QLoRA, suggesting that the adaptive rank mechanism alone is not enough, and the integration of mixed-precision quantization is crucial.

D.7 Impact of 2-Bit Quantization and LoftQ Iterations

We have conducted additional experiments to explore the performance of LoftQ with 2-bit quantization and its variations across different numbers of iterations.

In these experiments, we used the NF2 variant from LoftQ, based on QLoRA’s NF4, to implement 2-bit quantization, since QLoRA does not natively support this low-bit quantization (as stated in the original paper and the GitHub repository). The 2-bit results in the LoftQ paper were also based on this NF2 variant. We fine-tuned the models using a 52k dataset, with the rank for LoftQ set to 16. The superscripts on LoftQ’s bit-width values represent the number of LoftQ iterations, with 0 iterations considered approximately equivalent to QLoRA (since QLoRA does not provide a 2-bit quantization type).

The results of our experiments are summarized in Table 8.

Table 8: Performance comparison for 2-bit quantization and LoftQ iterations on LLaMA3.1-8B with 52k fine-tuning dataset. Superscripts on LoftQ bits indicate the number of initialization iterations. Accuracy is reported as %

Method	Bit-width	MMLU	GSM8K	ARC(C)	ARC(E)	BoolQ	HellaS	OBQA	PIQA	WinoG
LoftQ	2 ⁰	23.76	0.00	26.24	25.25	37.83	26.86	29.40	52.55	49.18
LoftQ	2 ¹	24.71	0.00	25.17	25.25	37.83	25.73	29.20	51.58	49.33
LoftQ	2 ⁵	24.65	0.00	25.17	24.83	37.83	26.30	28.20	51.41	49.41
LoftQ	2 ¹⁰	24.80	0.00	26.02	25.25	37.83	26.53	29.80	52.83	48.86
QR-Adaptor	3.625	62.58	0.53	55.93	82.43	82.13	79.23	45.60	81.83	74.79

Key Observations

- **MMLU Performance:** For the MMLU dataset, which involves multiple-choice questions, models with 2-bit quantization perform at approximately 25% accuracy, which is close to random guessing. Thus, LoftQ’s 2-bit quantization yields little practical improvement for MMLU on LLaMA3.1. This suggests that the performance of LoftQ with 2-bit quantization is not robust on complex tasks.

- **GSM8K Performance:** On the GSM8K dataset, LoftQ’s 2-bit quantization fails to provide any meaningful performance, resulting in 0% accuracy. This highlights the challenges of quantizing LLaMA3.1 to such low precision, especially on complex question-answering tasks.
- **Common Sense Reasoning Tasks:** For simpler reasoning tasks like WinoGrande, the LoftQ 2-bit quantized models show some capacity to answer, but there is no significant difference across LoftQ’s iterations, and the models still perform similarly to random guessing on most datasets.
- **QR-Adaptor Optimization:** For QR-Adaptor, we optimized based on theoretical memory savings from 4-bit quantization. Since 2-bit quantization does not reduce memory usage effectively, we used the theoretical savings in our optimization process. This optimization allowed QR-Adaptor to achieve better performance even when compared to LoftQ with 2-bit quantization.

Conclusion

From these results, we observe that LoftQ’s 2-bit quantization shows poor performance across the board. Even with multiple iterations (up to 10), LoftQ struggles to achieve reasonable accuracy on tasks like MMLU and GSM8K. In contrast, QR-Adaptor, with its unified optimization of both rank and bit-width during fine-tuning, consistently outperforms LoftQ and other methods.

Notably, while LoftQ’s 2-bit quantization performs poorly, QR-Adaptor manages to retain much better performance by leveraging the advantages of mixed-precision quantization, making it a more effective solution for LLaMA3.1. These findings suggest that for models requiring high precision, such as LLaMA3.1, extreme quantization to 2-bit precision may not be viable, and more moderate bit-widths, as used by QR-Adaptor, provide better results.

We hope these results contribute to the ongoing discussions in the community regarding effective quantization strategies and provide further insights into the practical use of quantized models.

E Version of LLMs

We provide the Hugging Face link of LLMs used in the experiment: LLaMA2-7B: <https://huggingface.co/NousResearch/Llama-2-7b-hf>; LLaMA2-13B: <https://huggingface.co/NousResearch/Llama-2-13b-hf>; LLaMA3.1-8B: <https://huggingface.co/meta-llama/Llama-3.1-8B>.

F More Implementation Details

In optimizing the pruned Llama2-7B model, a carefully designed hyperparameter configuration has been implemented to strike a balance between model performance and computational efficiency. The model is fine-tuned using a learning rate of 3×10^{-4} , with a batch size of 128, divided into micro-batches of 4 to effectively manage memory limitations. Input sequences are capped at 256 tokens, and a dropout rate of 0.05 is applied to the LoRA layers, specifically targeting the query, key, value, and output projections, as well as the gate, down, and up projections. Layer-specific quantization is applied at both 4-bit and 8-bit levels, optimizing memory usage while maintaining computational accuracy. The training is performed using the paged AdamW optimizer with 32-bit precision, ensuring both stability and efficiency. These settings have been rigorously tested and refined through the Optuna framework to achieve an optimal balance between model performance and resource efficiency.

G More Ablation

We conducted comprehensive ablation studies to evaluate the impact of initialization metrics and the sensitivity of the proposed Pareto Ranking Genetic Algorithm (PRGA) to key hyperparameters, including iteration counts and population size. These experiments aim to further substantiate the effectiveness of our proposed approach.

G.1 Gradient Norms vs. Relative Entropy

To assess the efficacy of initialization metrics, we compared the use of gradient norms and relative entropy in quantifying layer importance for fine-tuning quantized LLMs. The experimental results are summarized in Table 9.

Table 9: Comparison of gradient norms and relative entropy as initialization metrics on Llama2-13B. Bold values indicate the best performance for each task. Accuracy is reported as %

Initialization Metric	BoolQ	PIQA	HellaS	WinoG	ARC(E)	ARC(C)	OBQA	Average
Gradient Norms	80.79	80.13	79.16	71.69	78.72	50.97	45.40	69.51
Relative Entropy	81.08	80.83	79.80	71.98	79.13	51.65	45.60	70.07

Insights:

- **Limitations of Gradient Norms:** Gradient norms exhibit limited variability and are prone to biases induced by quantization, which undermines their reliability as an initialization metric for quantized models.
- **Advantages of Relative Entropy:** Relative entropy captures task-specific layer importance more effectively, resulting in robust initialization and improved performance in downstream optimization.

G.2 Sensitivity to Iteration Counts and Population Size

To analyze the sensitivity of PRGA to hyperparameters, we systematically varied the number of iterations and population sizes. Table 10 presents the results of these experiments.

Table 10: Sensitivity analysis of PRGA under different iteration counts and population sizes on Llama3.1-8B. Bold values indicate the best configuration.

Iterations	Population Size	Average Improvement (%)	Total Time (min)
5	3	+0.8	120
5	5	+1.2	150
10	5	+1.5	225
5	20	+1.6	375
10	20	+2.3	450

Insights:

- **Trade-offs in Population Size:** Smaller population sizes (e.g., 3) reduce computational cost but may fail to adequately explore the search space. Larger population sizes (e.g., 20) improve exploration and convergence but increase computational overhead.
- **Impact of Iteration Count:** Increasing the number of iterations improves optimization quality, as reflected in better Pareto fronts. However, the marginal benefits diminish beyond 10 iterations, indicating limited practical gains for further increases.
- **Balanced Configuration:** A population size of 5 and 5 iterations strikes a balance between performance improvement and computational efficiency. This configuration can be adjusted based on specific resource availability or performance requirements.

H Reproducibility Statement

To ensure the reproducibility of our results, we provide comprehensive documentation on the steps required to replicate our experiments. Our code is available in scripts such as `optuna_main-v3.py`, `post_training_mixed_quant.py`, and `run_optuna.py`, which handle hyperparameter optimization, mixed-precision quantization, and evaluation. For data preparation, we utilize the Alpaca Cleaned Dataset from `yahma/alpaca-cleaned`, which is automatically downloaded and processed using the `datasets` library. Our environment setup requires an NVIDIA GPU with

CUDA support, preferably with at least 20 GB of memory for the Llama2 model, as well as Python 3.8+ and dependencies like PyTorch, Transformers, Optuna, BitsAndBytes, PEFT, and other libraries, which can be installed via the `requirements.txt` file. The model we fine-tune is the Llama2 architecture (NousResearch/Llama-2-7b-hf), using a mixed-precision quantization approach via `bitsandbytes` and Low-Rank Adaptation (LoRA) with the `peft` library. The training is conducted using a mixed-precision setup where the model’s dtype is set to `torch.bfloat16` to optimize memory usage and computation efficiency. Our hyperparameter optimization framework leverages Optuna to maximize model accuracy while minimizing memory usage, tuning parameters like quantization bits (4 or 8 bits) and LoRA ranks (2 to 16). To replicate our training process, researchers can execute the provided scripts using the specified command-line arguments, which configure the model, output directories, number of trials, and evaluation tasks. Model checkpoints and Optuna results are saved at regular intervals. The training is conducted using the Hugging Face `Trainer`, configured with parameters including a batch size of 4, gradient accumulation steps of 16, warmup steps of 100, and a learning rate of $1e-4$, with evaluation and model saving steps set to every 200 steps. Evaluation is conducted using the `lm_eval` library, where metrics such as accuracy are recorded and saved in JSON format. All hyperparameter settings and model configurations are logged in the output directory, along with training progress and memory usage. Random seeds are set to ensure deterministic behavior. By following these steps, including hardware and software specifications, and running the scripts with the provided configurations, researchers can reproduce our experiments and validate the findings related to mixed-precision quantization and parameter-efficient fine-tuning.

I Ethics Statement

This work builds upon pre-trained large language models Llama2 and utilizes publicly available datasets for instruction fine-tuning Alpaca-clean. We do not introduce any new datasets or data collection processes, and therefore do not involve human annotation in this research. Additionally, our study focuses on improving model efficiency through pruning and quantization techniques, without engaging with sensitive content or user-specific data. As such, this paper does not present any ethical concerns beyond those already associated with the broader body of research on large language models and their datasets. All datasets and models used comply with their respective licenses and terms of use.

J Limitation

A constraint of our framework is the relatively long search time required to determine optimal task-specific configurations. This extended duration is necessary to ensure the best fine-tuning setup for each task. We recognize this as a current limitation and are actively working on improving the efficiency of our search algorithm.